Available online at www.ijournalse.org

**Emerging Science Journal**

(ISSN: 2610-9182)

Vol. 10, No. 3, June, 2026

# Application of New Type UHF Sensor for Partial Discharge Measurement in Air Insulated Switchgear

Muhammad Kodrat [1, 2*], Jean Pierre Uwiringiyimana [3], Umar Khayam [4, 5]

[1] *School of Electrical Engineering, Telkom University, Bandung 40257, Indonesia.*

[2] *Center of Excellence for Sustainable Energy and Climate Change, Telkom University, Bandung 40257, Indonesia.*

[3] *Center for Advanced Power Systems (CAPS), Florida State University, Tallahassee, FL 32310, United States.*

[4] *School of Electrical Engineering and Informatics, Institut Teknologi Bandung, Bandung 40132, Indonesia.*

[5] *Graduate School of Multidisiplinary Science and Technology, Institut Teknologi Bandung, Bandung 40132, Indonesia.*

**Abstract**

Accurate detection of partial discharge (PD) is crucial for monitoring high voltage (HV) and medium voltage (MV) of electrical power assets. Among the various methods used for partial discharge (PD) monitoring, ultra-high-frequency (UHF) monitoring is particularly advantageous for on-site/online applications due to its anti-interference and noise-canceling capabilities. Therefore, this study aimed to focus on the application of an ultrawideband antenna, operating between 0.9 to 4 GHz frequency range, for detecting PD defects in air-insulated switchgear. Specifically, the proposed ultrawideband antenna was designed, optimized, and fabricated on FR4 substrate with a thickness of 1.6 mm and dielectric constant of 4.4. To evaluate the sensitivity performance of the antenna, laboratory experiments were conducted using a PD protrusion model located inside a test chamber. Subsequently, the results were evaluated through waveform analysis, PD power spectrum analysis, scalogram analysis in both the time as well as frequency domains, and finally, the phase-resolved PD (PRPD) pattern analysis. The experimental results show that the proposed UHF antenna could detect PD signals with high sensitivity and high signal-to-noise ratio (SNR) when placed at 120 cm from the source. This implied that the proposed antenna was a suitable sensor for detecting PD in HV and MV air-insulated switchgear.

**Keywords:**
Partial Discharge;
Ultra-High Frequency;
Air Insulated Switchgear;
Power Spectrum PD;
Phase Resolved Partial Discharge.

**Article History:**

| | | | |
|---|---|---|---|
| **Received:** | 16 | July | 2025 |
| **Revised:** | 27 | April | 2026 |
| **Accepted:** | 13 | May | 2026 |
| **Published:** | 01 | June | 2026 |

## 1- Introduction

Power grid apparatuses perform an important role in power generation, power transmission, and power distribution. One of the critical components of high voltage (HV) and medium voltage (MV) power equipment is electrical insulation. Moreover, any fault in the insulation system may lead to a high electric field, which can eventually cause a partial discharge (PD) when the electrical device is subjected to high-voltage stress. The occurrence of PD in HV or MV assets is believed to be a main indicator of insulation aging and degradation, which, when not detected at an early stage, may lead to failure and breakdown. Examples of the main components of an electric power grid that may fail due to insulation problems include transformers, power cables, electric generators and motors, circuit breakers, power line insulators, and switchgear. Therefore, PD monitoring of the power equipment (HV and MV) should be performed in real-time and continuously to prevent premature failure as well as maintain safe operation and reliability.

Switchgear is an electrical device that includes disconnect switches (fuses or circuit breakers), earth switches, surge arresters, busbars, etc., whose main function is to control, protect, and isolate electrical equipment from the grid.

* **CONTACT**: muhammadkodrat@telkomuniversity.ac.id

**DOI:** https://doi.org/10.28991/ESJ-2026-010-03-014

Depending on the system voltage, switchgear can be operated with high and medium voltages. In addition, there are two well-known types of switchgear, namely Gas Insulated Switchgear (GIS) and Air-Insulated Switchgear (AIS). GIS uses sulfur hexafluoride gas ($SF_6$ ) as an insulating material, while AIS uses air as an insulating material. The two types of switchgear have different advantages and disadvantages. In terms of area, GIS installations require a smaller area than AIS installations. Meanwhile, in the aspect of maintenance, GIS is superior with a maintenance period of up to 25 years. This duration is in contrast with AIS, which requires maintenance every two years [1]. Currently, there is a need for electrical power equipment that supports sustainable and environmentally friendly development, particularly electricity generation and transmission as well as distribution. GIS has several advantages, but $SF_6$ gas used in GIS contributes to environmental pollution due to the impact on the greenhouse effect [2, 3]. Therefore, in this context, many studies regarding GIS insulation aim to find alternatives to environmentally friendly insulating gas that can reduce or even completely replace the use of $SF_6$ gas [4, 5].

AIS is a solution for optimizing the reliability of electricity systems. In recent years, 10 kV AIS has become a popular study topic [6], as it is believed to be able to replace the work function of switchgear in MV range in electricity distribution systems [7]. Studies have shown that AIS requires major modernization to maintain reliability and prevent damage. Typically, damage to AIS is similar to other electrical equipment, caused by air insulation in the system [8], [9]. AIS failure can also be caused by several factors, including operating at high voltage and high electric fields, thereby increasing the insulation temperature of the conductor material and there is also human error when maintaining the device. Other types of defects occur in air switchgear due to particle pollution, protrusion, and aging insulation. The impact of this defect causes fatal damage to the air switchgear insulation system [10, 11].

Damage caused by various defects in the insulation system of electrical power equipment is usually from PD phenomena. Conceptually, PD can be defined as a partial electric breakdown of a small portion of electrical insulation between two conductors, which under high voltage loads, can lead to degradation and failure of the insulation and eventually breakdown of the power supply equipment. Furthermore, insulation can be damaged because the insulating material is no longer able to withstand high electric fields due to defects in the system. Another cause that can lead to failure is the age of the material, which is susceptible to PD activity [12]. Therefore, for a reliable electrical power system, PD phenomena should be avoided or detected early before failures and losses occur in the electric power system. In this regard, by using PD monitoring technology as condition-based maintenance, it is necessary to evaluate the condition of the switchgear insulation system to prevent insulation failure or premature breakdown related to unplanned outages and equipment loss. It is crucial to be aware that the PD phenomenon is one of the issues that may occur in switchgear when left unchecked, thereby leading to device breakdown. In addition, PD in electrical equipment occurs in every type of insulation system, namely liquid, solid, and gas insulation. Furthermore, it is classified based on the type of defect insulation used. Following this, PD is usually classified into surface discharge, void discharge, and corona discharge [13].

PD causes various phenomena in different forms of energy, including light, sound (pressure waves), impulse currents, electromagnetic waves, and chemical effects [14–16]. This implies that highly sensitive and accurate PD detection technologies are required. It is important to note that PD can be detected using various sensors installed on high-voltage (HV) and medium-voltage (MV) power equipment. These include the conventional electrical method specified in the IEC 60270 standard, in which the PD sensor consists of a coupling capacitor connected to a measuring impedance. PD can also be detected using non-conventional methods, such as acoustic techniques employing acoustic sensors [17], as well as high-frequency (HF), very-high-frequency (VHF), and ultra-high-frequency (UHF) methods, which primarily utilize antennas [18–20].

The UHF method detects partial discharges by capturing the electromagnetic signals emitted by PD activity within the insulation system of electrical power assets. Compared with other methods, the UHF technique offers the advantage of detecting PD without requiring the power equipment under test to be de-energized. This differs from traditional electrical methods, which require a galvanic connection to the equipment being tested [21–23]. Therefore, the UHF technique is considered a non-invasive method, where PD pulses can be coupled through internally or externally mounted UHF sensors. For safety reasons, particularly in online PD monitoring applications, UHF sensors can be installed at a certain distance from the device under test. Previous studies [24, 25] on the application of the UHF method using UHF antennas continue to expand due to their ability to detect PD pulses with a high signal-to-noise ratio (SNR) while effectively suppressing ambient noise, especially in online and on-site PD monitoring. Table 1 presents examples of UHF antenna designs and applications reported in the literature.

PD detection technology can also be applied in AIS, similar to other power systems. Commonly used sensors in AIS include high-frequency current transformer (HFCT) sensors, impedance detectors, transient earth voltage (TEV) sensors, Rogowski coils, and UHF antennas. Furthermore, Hussain et al. [6] performed PD detection in AIS using unconventional methods with various types of PD sensors. In their study, the researchers employed a Rogowski coil sensor, a high-

frequency electric-field (E-field) sensor (D-point), and a loop antenna to detect partial discharges. All sensors were connected to a supervisory control and data acquisition (SCADA) system as a condition-monitoring platform for real-time observation of PD activity.

In Kluge and Lasica [26], PD activity in AIS was detected using HFCT and TEV sensors. Meanwhile, Sreeram et al. [27] detected transient voltage activity occurring in vacuum interrupter switchgear using a TEV sensor mounted on the metal wall of the switchgear enclosure. The studies conducted by Tan et al. [11] and Tan et al. [12] utilized impedance-detecting sensors to identify partial discharges in 10 kV air-insulated switchgear. In these investigations, a protrusion model was embedded inside the air-insulated switchgear to generate corona discharge activity, which eventually led to AIS degradation. Nevertheless, there remains a need to develop more sensitive UHF antennas for PD detection in both GIS and AIS applications.

This study aimed to design a UHF sensor (antenna) with ultra-wideband characteristics and use it to detect PD in AIS. The proposed UHF antenna was a microstrip antenna that was widely used in GIS and transformers, as shown in Table 1. Furthermore, this antenna was used to detect PD activity in a laboratory environment using an air-insulated test cell (chamber). To generate PD activity in the air-insulated test cell, a protrusion defect (needle-level electrode model) was installed in the center of the test cell as a PD source. During this experiment, the proposed UHF ultra-wideband antenna was positioned 120 cm from the PD source to detect the irradiated electromagnetic waves caused by PD activity. Additionally, the contribution of this work is in the application of microstrip-type ultra-wideband UHF in AC high-voltage AIS as an alternative PD sensor that could be used for PD monitoring in GIS and medium-voltage AIS. Following the application, PD measurements were performed using three voltage levels applied to the protrusion defect to produce discharge.

To validate and evaluate the sensitivity performance of the proposed UHF antenna in PD testing in AIS, HFCT sensor was used as a comparative PD sensor. The HFCT sensor is clamped on the ground cable to detect the PD pulse current flowing to the ground. To address the gaps in previous research, this paper presents a circular patch antenna design with a BNC connector for PD detection in air-insulated switchgear. This antenna is designed with a high operating frequency in the ultrawideband range. This UHF antenna is used to detect PD activity caused by fixed protrusion defects in AIS equipment. Experimental validation of PD detection capabilities focusing on magnitude, frequency spectrum, and PRPD shows that the proposed antenna effectively captures signals generated from PD while maintaining the desired performance in the operational frequency range, confirming the feasibility and practical value of PD parameters.

**Table 1. Studies about partial discharge detection using ultrawideband UHF sensor in high voltage equipment**

| UHF Sensor Designs | Material/Size | Medium | Bandwidth | References |
|---|---|---|---|---|
| Monopole coplanar | FR4/ 282 mm | Insulator | 0.4 – 3 GHz | Qi et al. [28] |
| Conical Monopole + radome | Teflon+ABS plastic/130 mm | GIS | 0.5 – 3 GHz | Yadam et al. [29] |
| Disk sensor internal | unknown/170 mm | GIS | 0.5 – 6.8 GHz | Yadam et al. [30] |
| CP Archimedean Spiral | FR4/158 mm | GIS | 0.5 – 5 GHz | Yadam et al. [31] |
| Planar monopole | FR4/314 mm | Transformer | 0.34 – 8 GHz | Do Nascimento Cruz et al. [32] |
| Slot spiral | FR4+teflon/100 mm | Transformer | 0.5 – 3 GHz | Ghanakota et al. [33] |
| Circular Microstrip | FR4/100 mm | Transformer | 0.9 – 4.4 GHz | Uwiringiyimana et al. [34] |
| Fractal Moore | FR4/ 65 mm | GIS | 0.3 – 3 GHz | Wang et al. [35] |
| Fractal Hilbert | FR4/ 80 mm | PD transformer model | 0.3 – 4 GHz | Salah et al. [36] |
| Antipodal Vivaldi | FR4/100 mm | Transformer | 0.8 – 3 GHz | Zhang et al. [37] |
| Fractal Hilbert | FR4/ 100 mm | PD transformer model | 0.35 – 3 GHz | Harbaji et al. [38] |

## 2- UHF Sensor: Design Characteristics and Fabrication

### *2-1- Research Methodology of UHF Sensor*

The research methodology, illustrated in Figure 1, outlines an approach that integrates computer-based simulations with experimental validation.

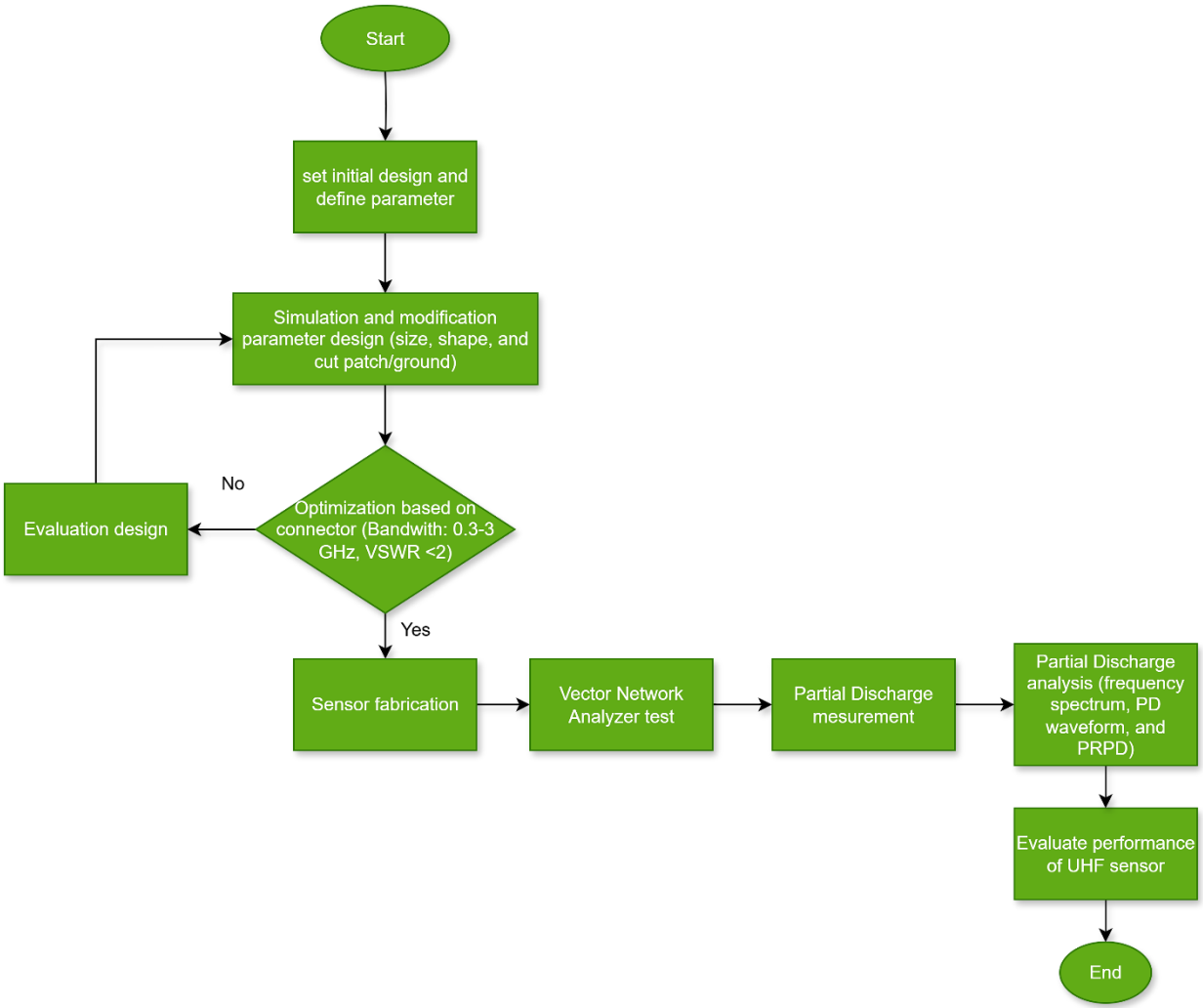


**Figure 1. Flowchart of UHF sensor research method**

### *2-2- Design Characteristics of Antenna*

Antenna design parameters are a set of fundamental technical characteristics that serve as benchmarks for performance and determine the physical shape of an antenna. The parameters involved in antenna design are interrelated and often must be understood in order to achieve the goal of detecting partial discharge signals. Some key parameters include antenna dimensions; resonance frequency, which determines the operating frequency band; impedance; gain; and VSWR. UHF antennas generally operate in the frequency range of 0.3 to 3 GHz, which is the same frequency spectrum for electromagnetic waves induced by PD. Based on this, the following basic antenna characteristics need to be adjusted when designing a UHF antenna that can detect the partial discharge frequency range.

#### *Size of UHF Antenna*

The size of the design is an important factor to consider when designing a UHF antenna. For UHF sensors used to capture electromagnetic waves emitted by PD, the antenna size must be adjusted based on the power apparatus to be applied. The design must be compact so that it can be integrated into the instrument device, while maintaining high directivity and sufficient gain and capturing partial discharge signals with a good signal-to-noise ratio (SNR).

#### *Bandwidth*

Bandwidth is the frequency range in which the antenna can still operate effectively with performance that meets certain criteria. This parameter indicates the extent to which the antenna can receive or transmit signals within a certain frequency range without experiencing significant power reflection. In the context of partial discharge (PD) measurement, a wide bandwidth is very important because PD signals are transient, covering a spectrum from hundreds of MHz to several GHz. Therefore, a UHF antenna with a wide bandwidth can capture more frequency components of the PD signal and increase the detection sensitivity to various types of PD activity in high-voltage insulation systems. To determine the bandwidth in antenna design, there are two types, fractional bandwidth and absolute bandwidth, as shown in Equations 1 and 2.

$$Fractional\ Bandwidth = \frac{f_h - f_l}{f_c} \times 100\% \quad (1)$$

$$Absolute\ Bandwidth = f_h - f_l \quad (2)$$

where, $f_h$, $f_l$, $f_c$ are the high frequency, low frequency, and center frequency, respectively. In addition, bandwidth is usually measured based on frequency operation with a return loss value below -10 dB.

***VSWR and Gain***

VSWR indicates that the antenna impedance is matched to the transmission line, typically 50 Ω, and the VSWR value ranges from 1 to infinity. VSWR < 2 means minimal reflection and efficient power transfer, while high VSWR indicates greater mismatch and energy loss due to reflection [39]. Equation 3 shows VSWR as a function of maximum and minimum voltage values and the reflection coefficient $|\Gamma|$. On the other hand, there is the Gain factor, which represents the antenna ability to direct or concentrate the transmitted power in a certain direction compared to the source. Gain combines both the antenna radiation direction and its efficiency, usually measured in decibels (dB). In partial discharge (PD) detection, achieving low VSWR over a wide frequency range ensures consistent signal coupling, while sufficiently high gain improves the reception of electromagnetic emissions from PD events.

$$VSWR = \frac{V_{max}}{V_{min}} = \frac{1+|\Gamma|}{1-|\Gamma|} \quad (3)$$

***Scattering Parameter ($S_{11}$) and Return Loss***

S-parameter and Return loss are factors in determining antenna design, as these two parameters are used to assess antenna performance in terms of power transmission efficiency and impedance matching. S-parameters ($S_{11}$), describe the ratio between reflected power and received power at the antenna port, and are used to determine the operating frequency and bandwidth of the antenna at values below -10dB. In the design of UHF antennas for partial discharge detection, low return loss and S11 values over a specific frequency range indicate that the antenna has optimal performance, with the ability to capture PD signals efficiently and with minimal power loss [40].

Return loss indicates how much power is reflected due to mismatches between the antenna and the transmission line, where a higher (more negative) value indicates that the antenna is working more efficiently with less power reflection. Equations 4 and 5 show the relationship between S11 and return loss.

$$S_{11} = 20 \log |\Gamma| \quad (4)$$

$$RL = -S_{11} = -20 \log|\Gamma| \quad (5)$$

The antenna used in the study was a UHF sensor that operated on a very wide band, which was called an ultra-wideband antenna. This antenna was a microstrip with a planar shape and was designed for partial discharge (PD) detection. Figure 2 presents the basic shape of the antenna, which consisted of the ground section, FR-4 dielectric substrate, patch, and feedline. The patch is connected to the coaxial cable via a feed line on the antenna. In addition, the antenna detected electromagnetic signals from PD sources, with the patch part of the antenna acting as a receiver for electromagnetic waves emitted by PD activity. Following this, the cable connected to the coaxial cable was in the form of a BNC connector. Apart from antenna design, optimization with various improvement methods on the connecting part also contributed to the performance results of the working frequency spectrum of the antenna [23]. Figure 2 presents the shape of the proposed antenna design with the following parameter dimensions. Substrate length (L) = 100 mm, substrate width (W) = 90 mm, circular patch radius (Rp) = 22.5 mm, feedline length (Lf) = 40 mm, supply line width (Wf) = 1.53 mm, ground plane length (Lg) = 37 mm and ground plane width (Wg) = 80 mm. Detailed information about the design, simulation, optimization, performance parameters, and testing of this antenna using a vector network analyzer could be found in Uwiringiyimana et al. [39].

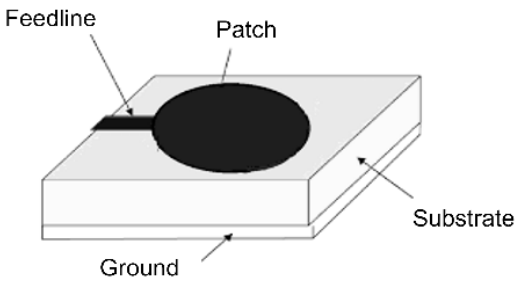


**Figure 2. General structure of microstrip UHF sensor**

### *2-3- UHF Sensor Fabrication*

The optimized version of the antenna design used for PD detection was printed using an FR-4 substrate with a thickness of 1.6 mm and a dielectric constant of 4.4. The ground parts, feedline, and patches were all made of annealed copper, which was a perfect conductor with a thickness of 0.035 mm. Furthermore, the antenna was manufactured with dimensions of 100 mm × 100 mm × 1.6 mm as shown in Figure 3. The voltage standing wave ratio (VSWR), reflection coefficient (S11), and antenna bandwidth were measured with a vector network analyzer (S5085 Copper Mountain) with a frequency range of 9 kHz to 8.5 GHz to evaluate the antenna sensitivity performance.

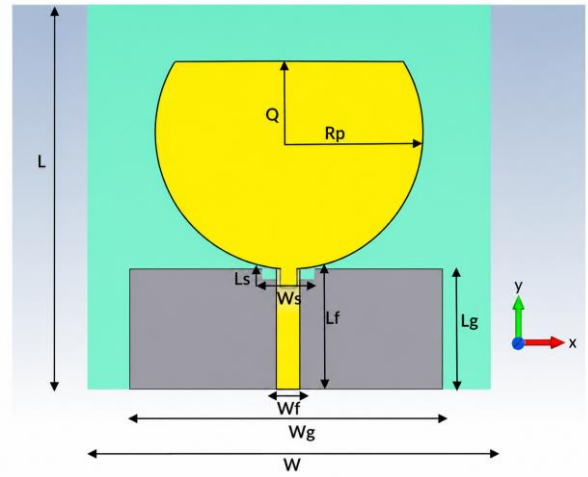


**Figure 3. Geometrical design of proposed ultrawideband UHF sensor**

Figure 4 shows the fabrication geometry of the proposed ultra-wideband antenna for PD detection. Figure 4-a presents the shape of a previously fabricated antenna that uses an SMA connector to connect a coaxial cable feedline. Furthermore, Figure 4-b presents a prototype antenna made by installing a BNC connector used for PD testing in this study. After redesigning the antenna, performance measurements were carried out using a vector network analyzer (VNA) in the laboratory by conditioning noise attenuation. In addition, the antenna sensitivity performance test was evaluated by reflection coefficient (return loss) and voltage standing wave ratio (VSWR) [21]. To assess whether the antenna functions well in PD detection, the designed antenna should have a wide bandwidth in the frequency range of 300 MHz to 3 GHz, a lower return loss of at least -10dB, and a lower VSWR of at least 2, where the working frequency [18]. As shown in Figure 5, the simulation and measurement results of the designed antenna were compared. As shown in Figure 5-a, the simulated and measured reflection coefficients were below -10 dB in the working frequency range of the antenna.

On the other hand, Figure 5-b, presents the comparison between the simulated and measured VSWR values. It could be seen that the designed antenna has a VSWR of less than 2 in the entire antenna frequency range. To improve antenna performance, BNC connector was used, comparing the measurement results obtained through the BNC connector with the SMA connector. Furthermore, The BNC connector was soldered directly to the antenna cable with tin material. By using BNC connector, the fabricated antenna had a higher number of resonant frequencies compared to antennas with an SMA connector. In addition, the use of BNC connectors led to a slight frequency shift towards lower frequencies compared to SMA connectors, as reviewed and compared in Table 2.

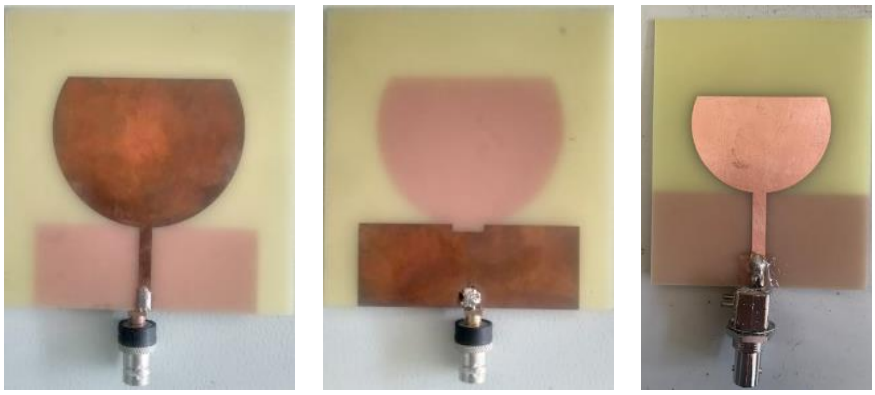

(a) (b)

**Figure 4. Fabricated ultrawideband UHF sensor with (a) SMA and (b) BNC connector**

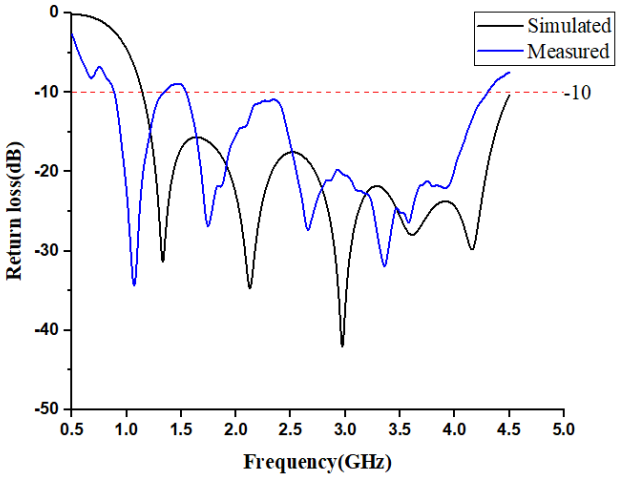


(a) Reflection coefficient of the designed ultrawideband antenna

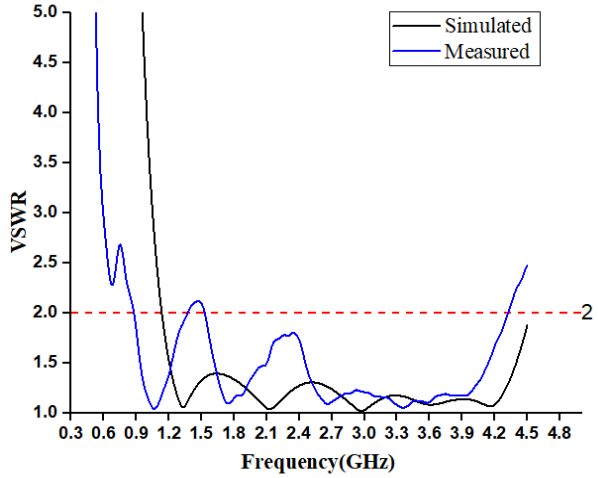


(b) VSWR of the designed ultrawideband antenna

**Figure 5. Simulated and Measured results of the fabricated antenna with the SMA connector**

**Table 2. Comparison between simulation and measurement results of the proposed ultrawideband antenna with SMA connector vs BNC connector**

| UHF Sensor Parameters | Antenna measurement | | |
|---|---|---|---|
| | Simulation | Measurement with SMA connector | Measurement with BNC connector |
| Fr1 | 1.3 GHz | 1.1 GHz | 0.9 GHz |
| Fr2 | 2.1 GHz | 1.7 GHz | 1.5 GHz |
| Fr3 | 2.9 GHz | 2.5 GHz | 1.7 GHz |
| Fr4 | 3.6 GHz | 3.4 GHz | 2.2 GHz |
| Fr5 | 4.1 GHz | - | 2.6 GHz |
| Fr6 | - | - | 2.8 GHz |
| Fr7 | - | - | 3.2 GHz |
| Fr8 | - | - | 3.5 GHz |
| Fr9 | - | - | 3.7 GHz |
| Rc1 | -31.3 dB | -35.3 dB | -18 dB |
| Rc2 | -34.0 dB | -27.6 dB | -30 dB |
| Rc3 | -41.8 dB | -26.4 dB | -30 dB |
| Rc4 | -27.0 dB | -31.2 dB | -40 dB |
| Rc5 | -29.3 dB | - | -36 dB |
| Rc6 | - | - | -38 dB |
| Rc7 | - | - | -48 dB |
| Rc8 | - | - | -42 dB |
| Rc9 | - | - | -32 dB |

* Fr = Frequency resonance, Rc = Reflection coefficient.

As shown in Table 2, the connector type may affect the bandwidth and resonant frequency of the antenna. Following through, antenna applications should be adjusted and planned with existing equipment [41]. Similarly, in the study conducted in Yadam et al. [29], n-type connectors were used as connectors to connect the antenna to the coaxial cable. BNC and SMA connectors have maximum frequency limits of 4 and 12 GHz, respectively. Selecting a BNC connector was a way to adapt the antenna application to existing equipment in the laboratory by using a coaxial cable that connects the antenna to the oscilloscope.

## 3- Experimental Setup

### *3-1- Artificial PD Defect*

Figure 6 illustrates a test cell or test chamber model used to represent an air-insulated switchgear model. To study the PD properties, a protrusion defect was developed as shown in Figure 6-a. Furthermore, the designed defect used a needle-plate model to represent the protrusion defect that produces a corona discharge at high electrical input. The needle was made of tungsten, having a length of 80 mm, and the needle electrode with a tip curvature of 0.3 mm needed to be connected to a high-voltage source. In addition, the electrode plate made of copper metal with a diameter of 50 mm and a radius of 3 mm should be connected to the ground.

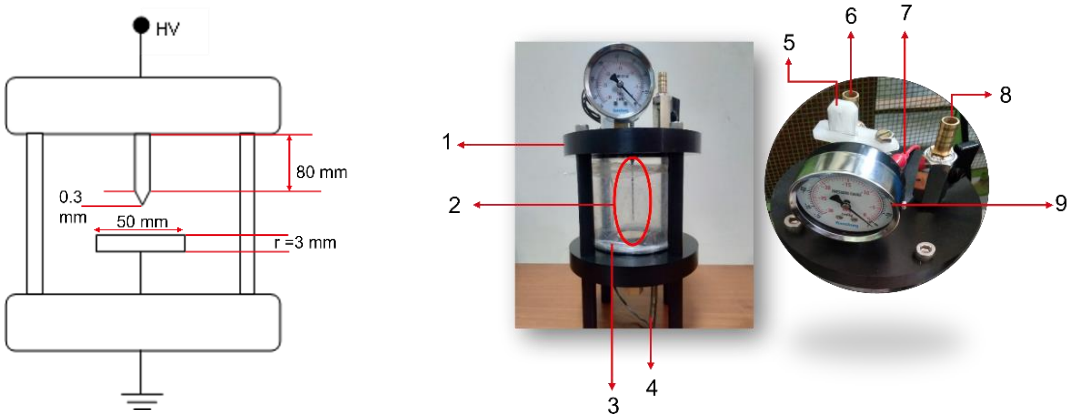


(a) (b)

**Figure 6. Defect protrusion model of air-insulated switchgear: (a) needle-plate, (b) structure of chamber:1 shell, 2 protrusion defects, 3 acrylic tubes, 4 ground, 5 gap distance setting, 6 gas inlet set, 7 HV conductor, 8 gas outlet set, and 9 vacuum pressure device.**

Figure 6-b presents the shape of the chamber used to generate partial discharge (PD) activity in air-insulated switchgear. Depending on the nature of the damage to the equipment, PD activity could be severe. For example, protrusions were critical defects that could occur in air and gas-insulated switchgear, causing insulation breakdown [10]. Therefore, in this study, a test cell chamber was designed with a needle plate model as a protrusion defect to produce corona discharge activity. The needle plate with a gap of 30 mm was installed in the chamber, as shown in Figure 6-b. The length of the chamber was 20 cm, the outer diameter 15 cm, and the inner diameter 12 cm. This test cell chamber was made of dielectric material, with the tube part made of acrylic glass. Additionally, the test cell chamber was equipped with other features such as a 1-30 mm gap adjustment, a vacuum pressure device, and a manual gas/air inlet/outlet setting.

### *3-2- PD Measurement Setup*

An experimental scheme for PD detection in air-insulated switchgear using a UHF ultra-wideband antenna was shown in Figure 7. The PD measurement circuit included a 220 V AC power source connected to a voltage regulator in the range of 0-220 V and a test transformer (100 kV/5 kVA). Furthermore, a protection resistor of 6.1 kΩ was used as a protection system to prevent damage to the transformer due to breakdown voltage, which may occur when high voltage is applied to the test object. A 100 pF coupling capacitor and a 40 nF voltage divider capacitor were installed in series, which sequentially functioned as a voltage pulse extractor and measured the output voltage of the transformer on an oscilloscope. In this experiment, a damaged protrusion (chamber) model was installed using a high-voltage source. The UHF sensor was placed at a certain distance near the room to detect electromagnetic waves emitted by PD activity in the test cell room. Additionally, a commercial HFCT sensor clamped around the ground wire was

simultaneously used to detect current pulses of partial discharge flowing to the ground. Both PD sensors, namely the proposed UHF ultra-wideband antenna and the HFCT sensor, were connected to a digital storage oscilloscope (DSO) via a 50-ohm coaxial cable.

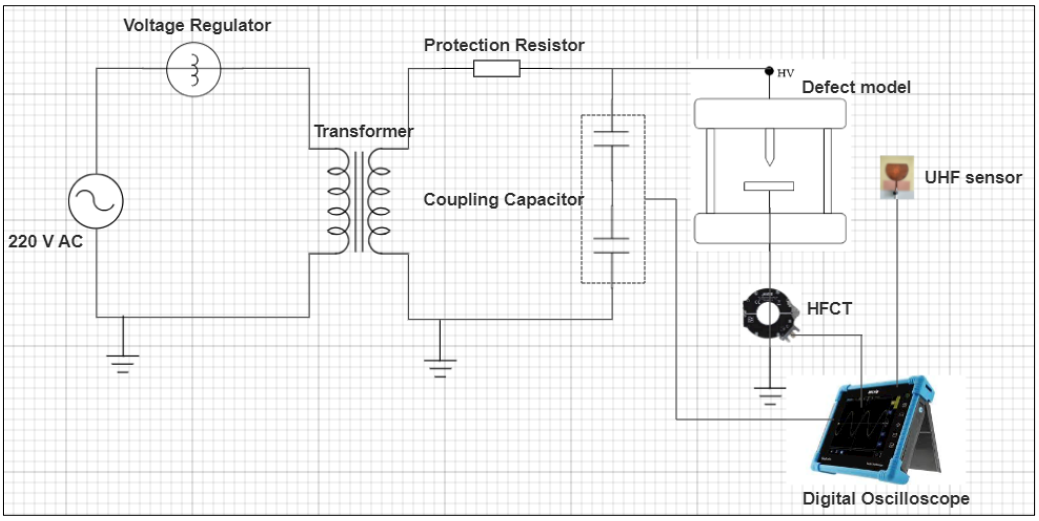


**Figure 7. Experimental setup used to generate corona discharge caused by a protrusion in air-insulated switchgear**

For the experimental procedure to evaluate PD detection with the proposed UHF sensor, the voltage was increased gradually from 0 kV until the first PD pulse occurred, which was referred to as partial discharge initial voltage (PDIV) which was observed to occur at 10 kV. The voltage was increased using a voltage regulator at increasing intervals, approximately 2 kV/s. Furthermore, the space was used as a model representation of the protrusions in air-insulated switchgear. Table 3 presents the PD test parameters determined during laboratory experiments. As shown in Table 3, the voltage value of 10 kV was determined as PDIV, the voltage at which the appearance of PD was first observed. In addition, to determine the sensitivity performance of the proposed UHF antenna in detecting PD activity at different applied voltages, PD measurements were conducted with three voltage variations, namely 12 kV, 14 kV as well as 16 kV, and each voltage fluctuation was used to obtain a PD dataset.

**Table 3. Experimental applied voltages to the test cell chamber under protrusion defect detected using the proposed UHF antenna**

| Voltage level | Applied voltage to the protrusion | Needle-plate gap distance | Antenna position from the chamber |
|---|---|---|---|
| Inception voltage I ($U_0$) | 10 kV | 30 mm | 120 cm |
| Voltage II (1.2 $U_0$) | 12 kV | | |
| Voltage III (1.4 $U_0$) | 14 kV | | |
| Voltage IV (1.6 $U_0$) | 16 kV | | |

In this PD measurement experiment, PD parameters such as time domain PD waveform, PD signal frequency spectrum, PD signal scalogram, and PRPD pattern were recorded as well as examined. To evaluate the characteristics of the PD pulses concerning the phase angle of the applied AC voltage, PRPD pattern analysis was performed using the PD pulses contained in 280 cycles of the applied sinusoidal voltage. When collecting PD data, all data were saved in the form of a CSV file. This file data became a large data set, which was then visualized and analysed.

## 4- PD Measurement: Result and Analysis

The sensitivity performance test results of the proposed UHF sensor were presented along with the results obtained using a commercial HFCT as a comparison partial discharge sensor. Before starting the PD test, the noise level (background noise) was measured in a high-voltage laboratory using the proposed UHF antenna and HFCT sensor. This process ensured there was a distinct difference between the actual PD signal and the noise [42]. Furthermore, background noise signals were detected when the power source was turned on. Figure 8 presents that the noise signal shape was read sequentially by the sensor. In Figure 8-a, the peak-to-peak voltage (Vpp) of the signal noise detected by the proposed UHF sensor is 11 mV, while the peak-to-peak voltage (Vpp) of the proposed UHF sensor detected the noise signal was 11 mV, and HFCT was 8 mV, as shown in Figure 8-b.

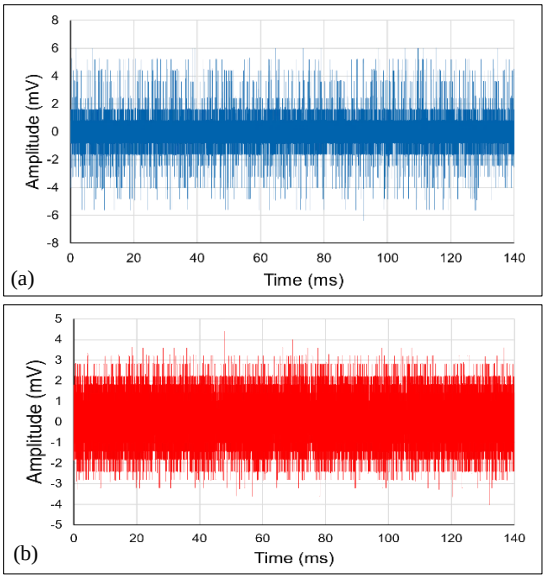


**Figure 8. Background noise captured by (a) the proposed UHF antenna, and (b) HFCT sensor**

### *4-1- Partial Discharge Waveform Analysis*

Figure 9 presents the PD waveforms detected by the proposed UHF sensor and HFCT sensing method in the time domain. The PD waveform signals were obtained from both sensors using three voltage levels of 12 kV, 14 kV, and 16 kV applied to the protrusion defect model. The PD signal was recorded using a digital storage oscilloscope and then processed. Figures 9-d to 9-f present the shape of the PD signal detected by the proposed ultra-wideband antenna. As shown in the figures by increasing the voltage applied to the protrusion defect, the amplitude of the UHF-PD signal detected by the proposed antenna also increased. Furthermore, by positioning the proposed antenna at a distance of 120 cm from the PD source, the antenna detected PD signals with peak-to-peak (Vpp) voltages of 25 mV, 72 mV, and 150 mV at three voltage variations of 12 kV, 14 kV, and 16 kV respectively. Additionally, the figure clearly presents that the proposed UHF ultra-wideband antenna could detect PD signals with high SNR even when placed further away from the test cell (PD source).

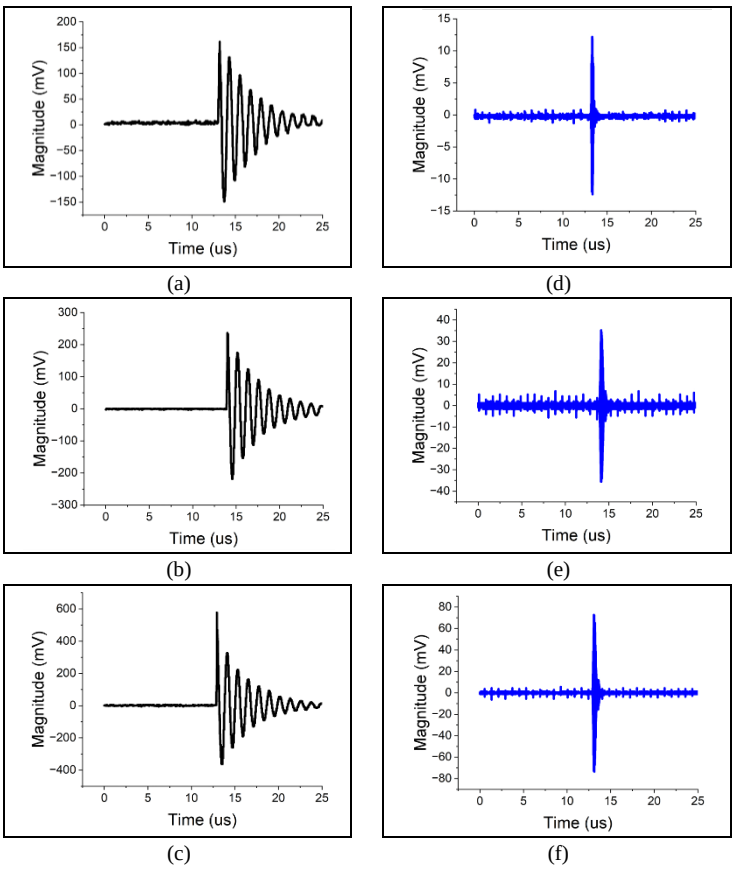


**Figure 9. PD waveform detected by HFCT sensor at an applied voltage of (a) 1.2 $U_0$, (b) 1.4 $U_0$, (c) 1.6 $U_0$ and ultrawideband antenna at an applied voltage of (d) 1.2 $U_0$ (e) 1.4 $U_0$ (f) 1.6 $U_0$.**

Figures 9-a to 9-c present the PD waveform signals acquired by a commercial HFCT sensor. At the applied voltage of 12 kV, 14 kV, and 16 kV, HFCT detected PD signals whose peak voltage magnitudes were 310 mV, 490 mV, and 950 mV respectively. This could be seen that the HFCT sensor identified PD signals with a higher power than those by the designed antenna. However, as previously explained, HFCT sensor was only used as a comparison sensor to detect PD signals and not to evaluate sensitivity because the PD detection method on the HFCT sensor was different from the UHF antenna. To explain the differences, the HFCT sensor detected PD current pulses flowing to the ground, and the UHF antenna identified electromagnetic waves emitted by PD activity [24, 25]. To further investigate the sensitivity performance of the proposed UHF antenna, a frequency spectrum analysis of the detected UHF PD signal identified by the designed UHF ultra-wideband antenna was provided in the next section.

Figure 10-a shows the average measurement results of partial discharge (PD) magnitude using a High-Frequency Current Transformer (HFCT) sensor. It can be seen that as the applied voltage increases from $1.2U_o$ (12 kV), $1.4U_o$ (14 kV), to $1.6U_o$ (16 kV), the PD signal amplitude increases significantly. The values of Vmin, Vmax, and Vpp increase from 150 mV, 170 mV, and 320 mV at $1.2U_o$ to 320 mV, 600 mV, and 920 mV at $1.6U_o$, respectively. This trend indicates that PD activity increases with increasing voltage, which indicates that the operating voltage level causes a stronger electric field in the insulation defect area, thereby increasing the frequency and energy of partial discharge. The HFCT sensor is capable of capturing these changes with high sensitivity to high-frequency impulse currents.

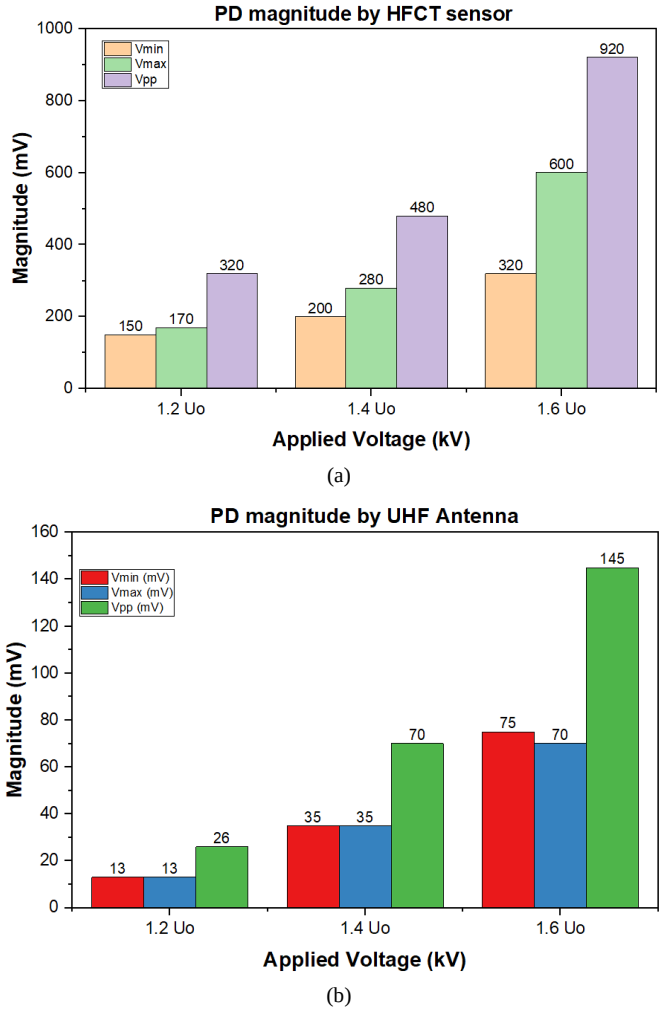


**Figure 10. Statistics of PD waveform parameters detected by (a) HFCT sensor, (b) UHF antenna**

Figure 10(b) shows the average magnitude of PD measurements using a UHF antenna. The increase pattern is similar to that of the HFCT sensor, but with a much smaller magnitude value. At $1.2U_o$, the Vpp value was recorded at 26 mV, then increased to 70 mV at $1.4U_o$, and reached 145 mV at $1.6U_o$. Although this increase is consistent, the amplitude of the PD signal received by the UHF antenna is lower because the antenna detects electromagnetic radiation emitted by PD discharge, not direct conduction current [34]. This makes the received signal weaker and dependent on the direction, distance, and sensitivity of the antenna to certain frequencies. In comparison, HFCT sensors show a much higher PD

magnitude than UHF antennas at every voltage level tested. This difference is due to different detection mechanisms: HFCT detects PD currents directly through conduction in the ground path, while UHF antennas capture electromagnetic signals that have been weakened by propagation in the air. However, UHF antennas are proposed to have the advantages of being non-invasive and free from direct electrical contact, making them a safe alternative for PD monitoring in enclosed spaces such as air-insulated switchgear. The combination of these two sensors can provide more comprehensive detection results and improve the accuracy of insulation condition diagnosis. The data presented shows the ability of UHF sensors to detect partial discharge signals emitted from AIS defect models.

### *4-2- Frequency Spectrum and Scalogram of PD Signals*

Figures 11 and 12 show the PD signal power spectrum for each voltage excitation level in the experimental PD model. The power spectrum presents the PD energy depending on the frequency. While the scalogram was a part of the tool that used the cross-wavelet transformation, this mode was used to represent the PD intensity scale concerning the PD pulse frequency and samples [30, 43, 44]. Figures 11 and 12 show the PD detection results using the HFCT sensor and ultra-wideband antenna in terms of power spectrum and scalogram visualization, respectively. The x-axis of the spectrum (right side) represented the frequency in GHz, and the y-axis signified the power spectrum (dB), while the left side of the figure was the PD scalogram visualization, where the x-axis was normalized time (samples) for 30 µs, the y-axis signified the frequency in GHz and the color in the image present the energy intensity of the PD signal.

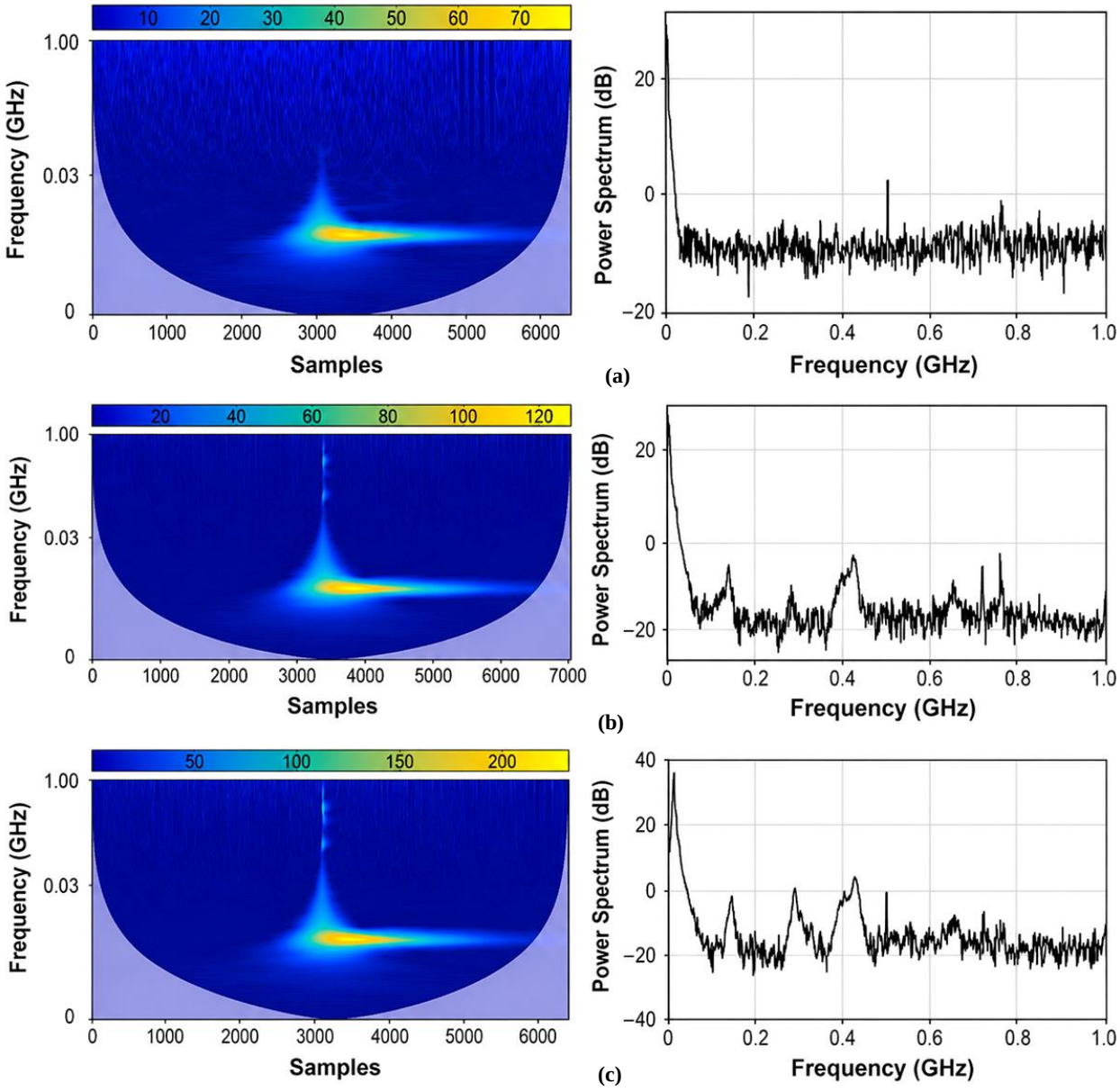


**Figure 11. Power spectrum (right side) and scalogram (left side) of PD signals detected by the HFCT sensor at applied voltages (a) 1.2 $U_0$, (b) 1.4 $U_0$, (c) 1.6 $U_0$**

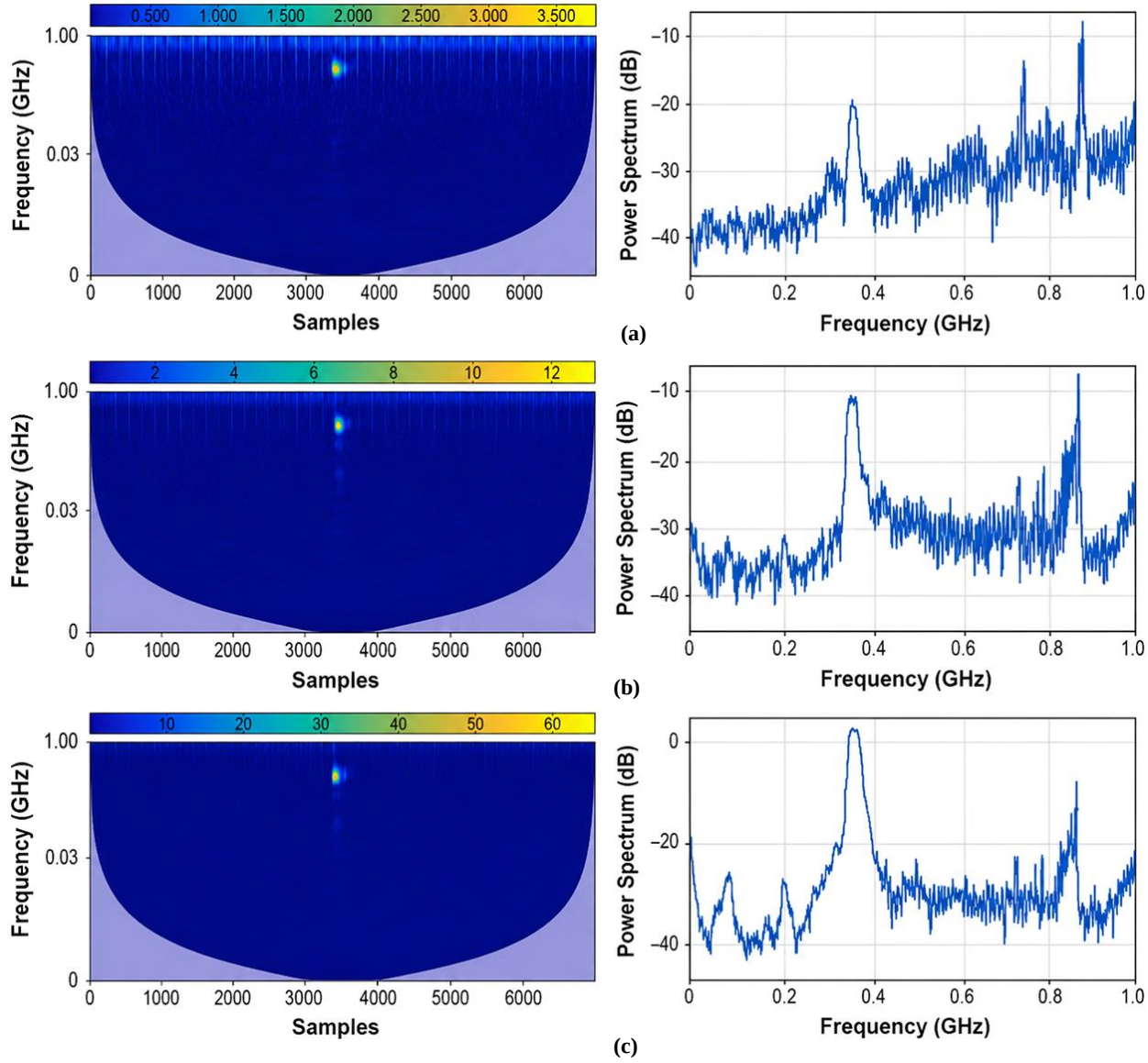


**Figure 12. Power spectrum (right side) and scalogram (left side) of PD signals detected by the proposed antenna at applied voltages (a) 1.2 $U_0$, (b) 1.4 $U_0$, (c) 1.6 $U_0$**

Figure 11 presents the visualization results of the power spectrum (right side) and scalogram (left side) for the PD signals detected by the HFCT sensor. The results show that, at test voltages of 12 kV, 14 kV, and 16 kV, the HFCT sensor identified PD signals with strengths of 20 dB, 25 dB, and 40 dB, respectively. The dominant frequency component of the PD signal remained concentrated around 21 MHz for all applied test voltages. In addition, this dominant frequency falls within the operating frequency range of commercial HFCT sensors (100 kHz–30 MHz). The scalogram shown on the left side of Figure 11 indicates that the main frequency components of the PD signal detected by the HFCT sensor were located between 0.01 and 0.03 GHz, confirming that the detected PD signals were within the operating bandwidth of HFCT sensors (100 kHz–30 MHz).

Figure 12 presents the PD detection results obtained using the developed ultra-wideband antenna in terms of the power spectrum (right side) and scalogram (left side). Based on the power spectrum analysis, at test voltages of 12 kV, 14 kV, and 16 kV, the proposed ultra-wideband antenna detected PD signals with power levels of −20 dB, −18 dB, and 3 dB, respectively. The main frequency components of the detected PD signals were consistently concentrated around 0.4 GHz and 0.85 GHz for all applied test voltages. Furthermore, the scalogram analysis shows that the PD energy intensity detected by the proposed ultra-wideband antenna was primarily concentrated around 0.85 GHz at all applied voltages. It can also be observed that the HFCT sensor detected a higher PD energy intensity than the proposed UHF antenna.

### *4-3- Phase Resolved Partial Discharge Patterns*

To further evaluate the PD characteristics in an air-insulated system using the proposed UHF antenna and a commercial HFCT sensor, a phase-resolved partial discharge (PRPD) pattern analysis was performed. PRPD was an

effective feature processing method to detect and identify various types of insulation defects. Furthermore, PRPD pattern analysis included information such as the number of PD, discharge amplitude (pC or mV), PD event cycle, and phase angle of the applied AC voltage. Several PD detection methods using PRPD have been documented in the literature for PD testing in laboratory experiments as well as for direct field applications.

In this study, the phase-voltage-number ($\varphi$-$u$-$n$) PRPD pattern method was used as a tool for evaluating the PD pattern of a protrusion model in an air-insulated test cell chamber. Figure 13 shows the PRPD pattern of the protrusion model obtained with the UHF antenna (right side) and HFCT sensor (left side). Additionally, the PRPD pattern data was collected from 280 cycles of applying a 50 Hz sinusoidal voltage. Before visualizing the PRPD pattern process, denoising was conducted on the raw PD signal data in the time domain. As seen in Figure 8, the background noise measurement results were useful for separating PD signal from the noise signal. Furthermore, the background noise peak voltage parameter was used as a threshold value to distinguish PD signals from noise signals, with any signal above the noise peak voltage being considered a PD signal.

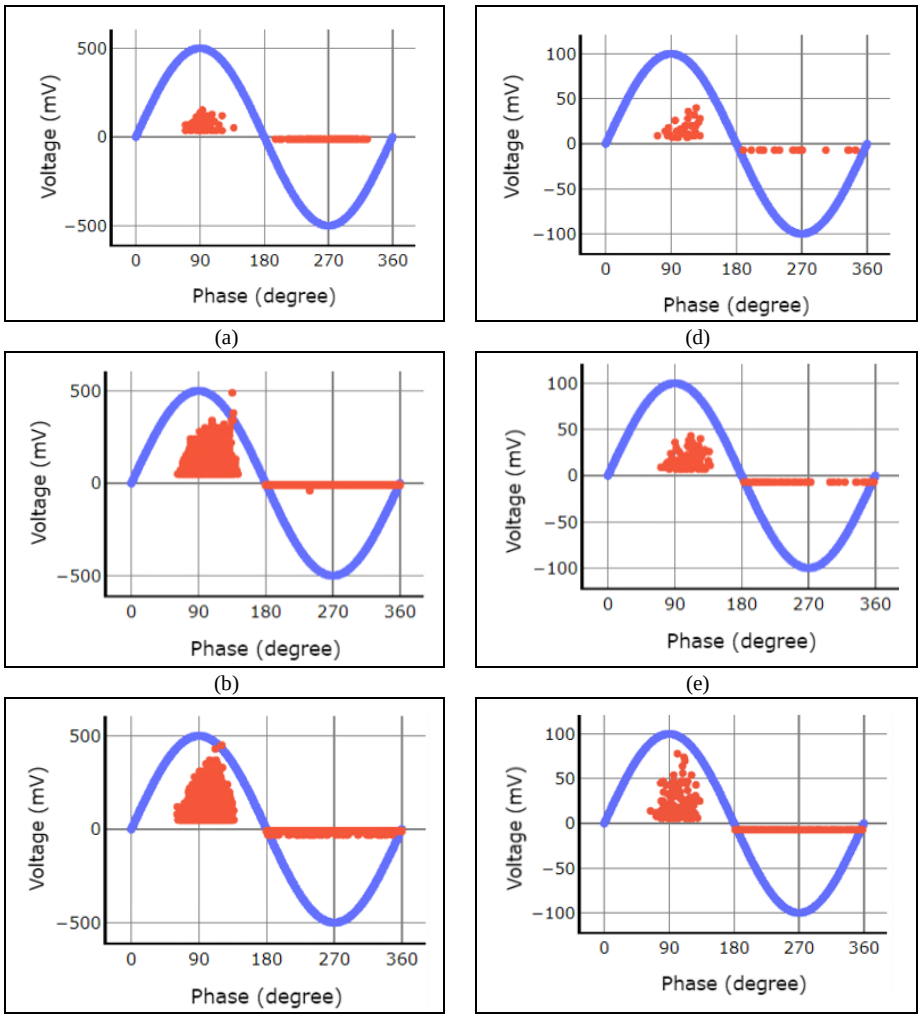


**Figure 13. PRPD patterns due to protrusion defect by HFCT under applied voltage levels of (a) 1.2 $U_0$, (b) 1.4 $U_0$, (c) 1.6 $U_0$, and by ultrawideband UHF antenna under applied voltage levels of (d) 1.2 $U_0$ (e) 1.4 $U_0$ (f) 1.6 $U_0$**

Figures 13-a to 13-c present the PRPD patterns for protrusion defects (corona discharge) detected by the proposed HFCT sensor at applied voltage levels of 12 kV, 14 kV, and 16 kV respectively, while Figures 13-d to 13-f show the PRPD patterns for the corona discharge detected by the designed ultra-wideband antenna. Based on the PRPD signature identified by both sensors, as shown in Figure 13, it was observed that the PD pulses with higher magnitudes were focused at the peak of the applied AC voltage at around a 90° phase angle in a positive half cycle, since the PD pulses in the negative cycle have lower, magnitude spreading from 180° to 360°, and therefore characterized the corona discharge pattern. The greatest discharge intensity occurred in the positive half cycle compared to the negative half cycle. In addition, by increasing the voltage applied to the test object, the number of PD pulses and the PD pulse amplitude detected by the UHF antenna and HFCT sensor also increased accordingly, specifically in the positive half wave.

Based on the activity that was described, it should be acknowledged that even HFCT sensors and UHF antennas have the same PRPD pattern. The HFCT sensor detected PD pulses with higher amplitude than those by the proposed UHF

antenna. As previously explained, the reason was that in this experiment the HFCT sensor was installed around the ground cable to detect the PD current flowing to the ground. This experiment was theoretically different from the UHF antenna which detected PD-induced electromagnetic waves compared to the UHF method [34, 44]. As shown in Figure 13, both sensors detect PD pulses whose patterns appeared the same in the positive and negative half cycles, showing how good the proposed UHF antenna was as an alternative PD sensor for diagnosing HV and MV power assets used. In general, diagnosis could be concluded that the proposed ultra-wideband antenna could detect PD defects in the same way as commercial HFCT sensors.

Table 4 presents the statistical results of Phase Resolved Partial Discharge (PRPD) measured using an HFCT sensor at various applied voltage levels, $1.2U_o$, $1.4U_o$, to $1.6U_o$. During the positive cycle, there is a significant increase in peak magnitude ($V_{max}$) when the voltage is increased from 12 kV to 14 kV, from 48 mV to 500 mV, respectively. This increase indicates that the intensity of partial discharge increases significantly with increasing voltage, while at 12 kV the air insulation dielectric is still categorized as having a low occurrence of PD. When the voltage is further increased to 16 kV, the peak magnitude decreases slightly to 490 mV, which may be due to changes in the discharge mechanism or dielectric erosion. However, in terms of the number of discharges, there is a large number of PDs in the positive cycle, as shown in Figure 13(c). For phase peak magnitude, the phase angle of the main PD shifts from 90º at 12 kV to 150º, indicating that PD tends to occur later in the positive cycle at higher voltages. The PD distribution in the positive cycle consistently occurs in the phase range of 80º to 120º at the lowest voltage, widening to 80º to 160º at higher voltages. The negative cycle shows PD characteristics that are much lower in intensity than the positive cycle. The peak magnitude in the negative cycle is much smaller, ranging only between 15 mV and 20 mV across the entire applied voltage range, and its increase with voltage is not the same as that in the positive cycle. This indicates that partial discharge is more dominant and stronger at positive polarity of the applied voltage. Meanwhile, the phase peak magnitude in the negative cycle shows that the main PD occurs in a very wide phase range, namely 180º to 350º at 12kV voltage and further widening to 180º to 360º at 14 kV and 16 kV applied voltages. The distribution of PD in the negative cycle also consistently occurs in a very wide phase range. This significant difference between the positive and negative cycles is characteristic of the type of air insulation corona discharge defect and indicates asymmetry in the partial discharge characteristics.

**Table 4. PRPD statistical result using the HFCT sensor**

| Applied Voltage | Positive Cycle | | | Negative Cycle | | |
|---|---|---|---|---|---|---|
| | Peak Magnitude, Vmax (mV) | Phase Peak Magnitude, Vmax (deg) | PD distribution (deg) | Peak Magnitude, Vmax (mV) | Phase Peak Magnitude, Vmax (deg) | PD distribution (deg) |
| 12 kV (1.2 $U_0$) | 48 | $90^0$ | $80^0 – 120^0$ | 15 | $180^0 – 350^0$ | $180^0 – 350^0$ |
| 14 kV (1.4 $U_0$) | 500 | $150^0$ | $80^0 – 160^0$ | 20 | $180^0 – 360^0$ | $180^0 – 360^0$ |
| 16 kV (1.6 $U_0$) | 490 | $150^0$ | $80^0 – 160^0$ | 20 | $180^0 – 360^0$ | $180^0 – 360^0$ |

Table 5 presents the statistical results of PRPD using the proposed UHF antenna at three voltage levels. In the positive cycle, an increase in voltage from 12 kV to 16 kV caused a significant increase in the peak amplitude of PD from 48 mV to 85 mV, indicating that the intensity of PD activity increased as the applied voltage increased. The peak phase angle is relatively constant at around 110°–120°, while the PD distribution is in the range of 80°–150°, indicating that PD activity mainly occurs in the early to mid-part of the positive cycle. In contrast, in the negative cycle, the peak amplitude remained low and stable at around 15 mV with a phase distribution between 180°–360°, indicating that the contribution of PD to the negative half-cycle was much smaller. Overall, this pattern shows the dominance of PD magnitude in the positive cycle, which becomes stronger with increasing voltage, consistent with the characteristics of partial discharge due to an increase in the local electric field on the positive side of the wave.

**Table 5. PRPD statistical result using the proposed UHF antenna**

| Applied Voltage | Positive Cycle | | | Negative Cycle | | |
|---|---|---|---|---|---|---|
| | Peak Magnitude, Vmax (mV) | Phase Peak Magnitude, Vmax (deg) | PD distribution (deg) | Peak Magnitude, Vmax (mV) | Phase Peak Magnitude, Vmax (deg) | PD distribution (deg) |
| 12 kV (1.2 $U_0$) | 48 | $120^0$ | $80^0 – 120^0$ | 15 | $180^0 – 360^0$ | $180^0 – 360^0$ |
| 14 kV (1.4 $U_0$) | 49 | $110^0$ | $80^0 – 150^0$ | 15 | $180^0 – 360^0$ | $180^0 – 360^0$ |
| 16 kV (1.6 $U_0$) | 85 | $110^0$ | $80^0 – 150^0$ | 15 | $180^0 – 360^0$ | $180^0 – 360^0$ |

Table 6 presents a comparison of various types of UHF antennas used for partial discharge signal detection, reviewed in terms of sensor type, size, bandwidth, return loss, and VSWR value. Based on the data, each antenna has different characteristics according to its design and application. Based on the presentation in Table 6, the antennas proposed in Uwiringiyimana et al. [45] and Kong et al. [46], namely planar rectangular and coplanar antennas, have relatively narrow bandwidths. The same applies to the antennas proposed in Dimitrov et al. [47], which still have relatively narrow

bandwidths. Meanwhile, the antenna designs proposed in Shams et al. [48] and Chen et al. [49] show a wider bandwidth coverage. The fractal antenna design has a wide bandwidth range, but most of the return loss values are below -24.49 dB, indicating good signal reflection performance. Meanwhile, the antenna resulting from this research (circular patch) shows competitive performance compared to other antennas. With a size of 100×80 mm, this antenna has a wide bandwidth range of 0.9–4 GHz, and a return loss of -30 dB at 1.5 GHz and -48 dB at 3.2 GHz, indicating excellent radiation efficiency. The VSWR value of 1.2 also indicates good impedance matching between the antenna and the measuring system, thereby minimizing reflected waves. Overall, this circular patch antenna provides the best combination of compact size, efficiency, and performance stability over a wide frequency range compared to other references

**Table 6. Comparison of different UHF antenna types**

| References | Sensor | Size | Bandwidth | Return loss at frequency work | VSWR |
|---|---|---|---|---|---|
| Uwiringiyimana et al. [45] | Planar rectangular antenna | 80×70 mm | 1.44 – 2.59 GHz | -31.6 dB 1.63 GHz<br>-26.8 dB 2.26 GHz | 1.06 |
| Kong et al. [46] | Coplanar antenna | 200×187 mm | 500 MHz-1120 MHz | -23 dB 500 MHz | 1.5 |
| Dimitrov et al. [47] | Spiral antenna | 10×46.6×59×65 mm (hybrid spiral) | 0.2 MHz – 1.8 GHz | -25 dB 1.6 GHz | Unknown |
| Shams et al. [48] | Fractal antenna | 100×100 mm | 1.7 – 3.3 GHz | -24.49 dB 1.17 GHz | 1.1 |
| Chen et al. [49] | Log periodic dipole array | 1460.7 $cm^2$ | 0.3 – 3 GHz | Unknown | 1.62 |
| **Present Study** | **Circular patch** | **100×80 mm** | **0.9 – 4 GHz** | **-30 dB 1.5 GHz<br>-48 dB 3.2 GHz** | **1.2** |

## 5- Conclusion

This study explored the PD properties of a protrusion defect model developed in an air-filled chamber. Experiments were conducted on a laboratory scale using an ultra-wideband UHF sensor simultaneously having a commercial HFCT sensor to detect PD models with protrusion defects, and the conclusions drawn were as follows: (1) The proposed UHF method used an ultra-wideband UHF antenna to detect PD activity in AIS with a protrusion defect. Specifically, the antenna was effective in detecting PD signals at a distance of 120 cm from the source. In addition, electromagnetic waves emitted by PD activity due to protrusion inside the air-insulated test chamber were detected accurately. (2) The study presents that PD signal parameters such as PD number and PD pulse size increased in proportion to the magnitude of the test voltage applied to the PD defect model. (3) According to the analysis of the PRPD pattern of the protrusion defects detected by the UHF antenna and HFCT sensor, there was an observation that the PD pulses at the peak of the applied AC voltage were at around a phase angle of 90° in the positive half cycle. Furthermore, the PD pulses were spread out in the negative half cycle from 180° to 360°, which characterized the corona discharge pattern due to the protrusion defect. The PRPD pattern of PD pulses detected by the HFCT sensor was almost similar to the PRPD pattern by the proposed ultra-wideband antenna; therefore, the proposed UHF antenna was able to identify types of defects in the insulation system of HV and MV electrical power equipment.

## 6- Declarations

### *6-1- Author Contributions*

Conceptualization, M.K. and U.K.; methodology, M.K.; software, M.K.; validation, U.K., J.P., and M.K.; formal analysis, J.P.; investigation, M.K.; resources, U.K.; data curation, J.P.; writing—original draft preparation, M.K.; writing—review and editing, J.P.; visualization, M.K.; supervision, U.K.; project administration, M.K.; funding acquisition, U.K. All authors have read and agreed to the published version of the manuscript.

### *6-2- Data Availability Statement*

The data presented in this study are available in the article.

### *6-3- Funding*

This work was supported in part by the Telkom University Research and Community Service Unit (PPM Tel-U); and in part by the Research, Community Service and Innovation Program (P2MI) funded by the School of Electrical Engineering and Informatics, Institut Teknologi Bandung, Indonesia.

### *6-4- Institutional Review Board Statement*

Not applicable.

### *6-5- Informed Consent Statement*

Not applicable.

### *6-6- Conflicts of Interest*

The authors declare that there is no conflict of interest regarding the publication of this manuscript. In addition, the ethical issues, including plagiarism, informed consent, misconduct, data fabrication and/or falsification, double publication and/or submission, and redundancies have been completely observed by the authors.

## 7- References


[1] Damiri, D. J., & Prasetio, T. W. (2021). Redesign Gas Insulated Switchgear to Semi Air Insulated Switchgear 500 kV side and 150 kV side in EHVS Kembangan. IOP Conference Series: Materials Science and Engineering, 1098(4), 042033. doi:10.1088/1757-899x/1098/4/042033.

[2] Beroual, A., Khaled, U., & Coulibaly, M. L. (2018). Experimental investigation of the breakdown voltage of $CO_2$, $N_2$, and $SF_6$ gases, and $CO_2$-$SF_6$ and $N_2$-$SF_6$ mixtures under different voltage waveforms. Energies, 11(4), 1–12. doi:10.3390/en11040902.

[3] Loizou, L., Han, Q., Chen, L., Liu, Q., Waldron, M., Wilson, G., Bautista, R. F., & Seltzer-Grant, M. (2022). Partial Discharge Characteristics of C3F7CN Gas Mixture Using the UHF Method. Energies, 15(20), 7731. doi:10.3390/en15207731.

[4] Chang, H., Sinha, N., Choi, H., Song, M. Y., Jang, H. J., Oh, Y. H., & Song, K. D. (2023). Theoretical process for the investigation of dielectric characteristics of F3NO as an alternative gas for $SF_6$. AIP Advances, 13(6), 065215. doi:10.1063/5.0147515.

[5] Franck, C. M., Chachereau, A., & Pachin, J. (2021). $SF_6$-Free Gas-Insulated Switchgear: Current Status and Future Trends. IEEE Electrical Insulation Magazine, 37(1), 7–16. doi:10.1109/MEI.2021.9290463.

[6] Hussain, G. A., Hummes, D., Zaher, A., Safdar, M., & Lehtonen, M. (2019). Hybrid Sensing of Partial Discharge Faults in Air Insulated Switchgear. Proceedings - 2019 IEEE International Conference on Environment and Electrical Engineering and 2019 IEEE Industrial and Commercial Power Systems Europe, EEEIC/I and CPS Europe 2019, 8783931. doi:10.1109/EEEIC.2019.8783931.

[7] Sun, G., Chen, S., Chen, B., Liu, Y., Chen, B., Li, H., Deng, R., & Fu, A. (2023). Study on Electromagnetic-Thermal Simulation of 10kV Air Insulated Switchgear. 2023 5th Asia Energy and Electrical Engineering Symposium, AEEES 2023, 378–383. doi:10.1109/AEEES56888.2023.10114076.

[8] Nascimento, F. de A. O., Coelho, R. D. A., Xavier, G. V. R., Alvim, P. D., Junior, A. C. D. S., & Silva, H. S. (2025). Wavefront Detection and Event Segmentation Method for Partial Discharge Signal Analysis. IEEE Access, 13, 111602–111613. doi:10.1109/ACCESS.2025.3582635.

[9] Suwarno. (2016). Partial discharge in high voltage insulating materials. International Journal on Electrical Engineering and Informatics, 8(1), 147–163. doi:10.15676/ijeei.2016.8.1.11.

[10] Tang, J., Yang, X., Ye, G., Yao, Q., Miao, Y., & Zeng, F. (2017). Decomposition Characteristics of $SF_6$ & Partial Discharge Recognition Under Negative DC Conditions. Energies, 10(4), 556. doi:10.3390/en10040556.

[11] Tan, Q., Song, B., Wang, L., & Wu, S. (2023). Study on characteristics gases of metal protrusions partial discharge in 10-kV air-insulated switchgear. IET Science, Measurement and Technology, 17(6), 221–229. doi:10.1049/smt2.12147.

[12] Tan, Q., Zhang, T., Wu, S., Gao, J., & Song, B. (2022). Diagnosis of Partial Discharge Based on the Air Components for the 10 kV Air-Insulated Switchgear. Sensors, 22(6), 1–11. doi:10.3390/s22062395.

[13] Shahsavarian, T., Pan, Y., Zhang, Z., Pan, C., Naderiallaf, H., Guo, J., Li, C., & Cao, Y. (2021). A Review of Knowledge-Based Defect Identification via PRPD Patterns in High Voltage Apparatus. IEEE Access, 9, 77705–77728. doi:10.1109/ACCESS.2021.3082858.

[14] Wu, M., Cao, H., Cao, J., Nguyen, H. L., Gomes, J. B., & Krishnaswamy, S. P. (2015). An overview of state-of-the-art partial discharge analysis techniques for condition monitoring. IEEE Electrical Insulation Magazine, 31(6), 22–35. doi:10.1109/MEI.2015.7303259.

[15] Hussain, M. R., Refaat, S. S., & Abu-Rub, H. (2021). Overview and Partial Discharge Analysis of Power Transformers: A Literature Review. IEEE Access, 9, 64587–64605. doi:10.1109/ACCESS.2021.3075288.

[16] Habib, B., Al Zaabi, O., Harid, N., Al Hosani, K., & Alkhatib, M. (2024). Condition Monitoring Based on Partial Discharge Diagnostics Using UHF Sensors: A Comprehensive State-of-the-Art Review. IEEE Transactions on Dielectrics and Electrical Insulation, 31(6), 2860–2873. doi:10.1109/TDEI.2024.3409517.

[17] Sikorski, W., & Wielewski, A. (2023). Low-Cost Online Partial Discharge Monitoring System for Power Transformers. Sensors, 23(7), 1–21. doi:10.3390/s23073405.

[18] Khayam, U., Suryandi, A. A., & Rachmawati. (2023). Design of Bowtie Antenna with Rounded Edge and Middle-Sliced Modifications for UHF Partial Discharge Sensor. IEEE Access, 11, 22822–22834. doi:10.1109/ACCESS.2023.3252006.

[19] Azam, K. M. K., Othman, M., Latef, T. A., Illias, H. A., Hossain, Z. K. M. Z., Yamada, Y., Kamardin, K., Alkhatib, M., Hussein, M. I., & Abidin, Z. Z. (2025). Standalone Identification Antenna for Resonator Tag-Free Far-Field Chipless RFID Sensors. IEEE Transactions on Antennas and Propagation, 73(9), 6914–6927. doi:10.1109/TAP.2025.3574862.

[20] Kaziz, S., Said, M. H., Imburgia, A., Maamer, B., Flandre, D., Romano, P., & Tounsi, F. (2023). Radiometric Partial Discharge Detection: A Review. Energies, 16(4), 1–33. doi:10.3390/en16041978.

[21] De Oliveira, A. C., Da Costa, E. G., Serres, A. J. R., Xavier, G. V. R., De Souza, V. C., De Almeida, A. C. A., Guedes, W. B., & Prisco, R. K. (2022). Application of Bioinspired Antennas in the Monitoring of High Voltage Circuit Breakers. IEEE Transactions on Power Delivery, 37(5), 4418–4426. doi:10.1109/TPWRD.2022.3170309.

[22] Xavier, G. V. R., De Oliveira, A. C., Silva, A. D. C., Nobrega, L. A. M. M., Da Costa, E. G., & Serres, A. J. R. (2021). Application of Time Difference of Arrival Methods in the Localization of Partial Discharge Sources Detected Using Bio-Inspired UHF Sensors. IEEE Sensors Journal, 21(2), 1947–1956. doi:10.1109/JSEN.2020.3019760.

[23] Xavier, G. V. R., Serres, A. J. R., da Costa, E. G., de Oliveira, A. C., Martins Nobrega, L. A. M., & de Souza, V. C. (2019). Design and application of a metamaterial superstrate on a bio-inspired antenna for partial discharge detection through dielectric windows. Sensors (Switzerland), 19(19), 4255. doi:10.3390/s19194255.

[24] Xavier, G. V. R., Silva, H. S., Da Costa, E. G., Serres, A. J. R., Carvalho, N. B., & Oliveira, A. S. R. (2021). Detection, classification and location of sources of partial discharges using the radiometric method: Trends, challenges and open issues. IEEE Access, 9, 110787–110810. doi:10.1109/ACCESS.2021.3102888.

[25] Azam, S. M. K., Othman, M., Illias, H. A., Abdul Latef, T., Tariqul Islam, M., & Fadzil Ain, M. (2023). Ultra-high frequency printable antennas for partial discharge diagnostics in high voltage equipment. Alexandria Engineering Journal, 64, 709–729. doi:10.1016/j.aej.2022.11.026.

[26] Kluge, P., & Lasica, A. (2022). Non-invasive PD measurement method in air-insulated switchgear - signal processing. 2022 23rd International Conference on Computational Problems of Electrical Engineering (CPEE), 1–4. doi:10.1109/CPEE56060.2022.9919651.

[27] Sreeram, V., Arunkumar, S., Reddy, S. S., Gurudev, T., & Maroti. (2022). Comparative Analysis of Transients in AIS and GIS With Vacuum Interrupters. IEEE Transactions on Plasma Science, 50(9), 2681–2686. doi:10.1109/TPS.2022.3202339.

[28] Qi, Y., Fan, Y., Bing, G., Jia, R., Sen, W., Wei, S., & Jadoon, A. (2019). Design of Ultra-Wide Band Metal-Mountable Antenna for UHF Partial Discharge Detection. IEEE Access, 7, 60163–60170. doi:10.1109/ACCESS.2019.2910211.

[29] Yadam, Y. R., Ramanujam, S., & Arunachalam, K. (2021). An Ultrawideband Conical Monopole with Radome for Detection of Partial Discharges. IEEE Sensors Journal, 21(17), 18764–18772. doi:10.1109/JSEN.2021.3090099.

[30] Yadam, Y. R., Sarathi, R., & Arunachalam, K. (2022). Numerical and Experimental Investigations on Influence of Internal Defect Parameters on Partial Discharge Induced UHF Signals in Gas Insulated Switchgear. IEEE Access, 10, 110785–110795. doi:10.1109/ACCESS.2022.3213690.

[31] Yadam, Y. R., Sarathi, R., & Arunachalam, K. (2022). Planar Ultrawideband Circularly Polarized Cosine Slot Archimedean Spiral Antenna for Partial Discharge Detection. IEEE Access, 10, 35701–35711. doi:10.1109/ACCESS.2022.3163303.

[32] Do Nascimento Cruz, J., Serres, A. J. R., De Oliveira, A. C., Xavier, G. V. R., De Albuquerque, C. C. R., Da Costa, E. G., & Freire, R. C. S. (2019). Bio-inspired printed monopole antenna applied to partial discharge detection. Sensors (Switzerland), 19(3), 628. doi:10.3390/s19030628.

[33] Ghanakota, K. C., Yadam, Y. R., Ramanujan, S., Vishnu Prasad, V. J., & Arunachalam, K. (2022). Study of Ultra High Frequency Measurement Techniques for Online Monitoring of Partial Discharges in High Voltage Systems. IEEE Sensors Journal, 22(12), 11698–11709. doi:10.1109/JSEN.2022.3172173.

[34] Uwiringiyimana, J. P., Khayam, U., Suwarno, & Montanari, G. C. (2022). Comparative Analysis of Partial Discharge Detection Features Using a UHF Antenna and Conventional HFCT Sensor. IEEE Access, 10, 107214–107226. doi:10.1109/ACCESS.2022.3212746.

[35] Wang, Y., Wang, Z., & Li, J. (2017). UHF Moore Fractal Antennas for Online GIS PD Detection. IEEE Antennas and Wireless Propagation Letters, 16, 852–855. doi:10.1109/LAWP.2016.2609916.

[36] Salah, W. S., Gad, A. H., Attia, M. A., Eldebeikey, S. M., & Salama, A. R. (2022). Design of a compact ultra-high frequency antenna for partial discharge detection in oil immersed power transformers. Ain Shams Engineering Journal, 13(2), 101568. doi:10.1016/j.asej.2021.08.011.

[37] Zhang, J., Zhang, X., & Xiao, S. (2017). Antipodal Vivaldi Antenna to Detect UHF Signals That Leaked Out of the Joint of a Transformer. International Journal of Antennas and Propagation, 2017(1), 9627649. doi:10.1155/2017/9627649.

[38] Harbaji, M. M. O., Zahed, A. H., Habboub, S. A., Almajidi, M. A., Assaf, M. J., El-Hag, A. H., & Qaddoumi, N. N. (2017). Design of Hilbert Fractal Antenna for Partial Discharge Classification in Oil-Paper Insulated System. IEEE Sensors Journal, 17(4), 1037–1045. doi:10.1109/JSEN.2016.2638804.

[39] Uwiringiyimana, J. P., Khayam, U., Suwarno, & Montanari, G. C. (2022). Design and Implementation of Ultra-Wide Band Antenna for Partial Discharge Detection in High Voltage Power Equipment. IEEE Access, 10, 10983–10994. doi:10.1109/ACCESS.2022.3144416.

[40] Khayam, U., Hamdani, Y. M., & Rachmawati. (2024). Design of Modified UWB Microstrip Antenna for UHF Partial Discharge Sensor. Emerging Science Journal, 8(5), 1716–1731. doi:10.28991/ESJ-2024-08-05-03.

[41] Tang, J., Jin, M., Zeng, F., Zhou, S., Zhang, X., Yang, Y., & Ma, Y. (2017). Feature selection for partial discharge severity assessment in gas-insulated switchgear based on minimum redundancy and maximum relevance. Energies, 10(10), 1–14,. doi:10.3390/en10101516.

[42] Ardila-Rey, J. A., Cerda-Luna, M. P., Rozas-Valderrama, R. A., De Castro, B. A., Andreoli, A. L., & Muhammad-Sukki, F. (2020). Separation techniques of partial discharges and electrical noise sources: A review of recent progress. IEEE Access, 8, 199449–199461. doi:10.1109/ACCESS.2020.3035249.

[43] Barrios, S., Buldain, D., Comech, M. P., & Gilbert, I. (2021). Partial Discharge Identification in MV Switchgear Using Scalogram Representations and Convolutional AutoEncoder. IEEE Transactions on Power Delivery, 36(6), 3448–3455. doi:10.1109/TPWRD.2020.3042934.

[44] Rodrigo Mor, A., Muñoz, F. A., Wu, J., & Castro Heredia, L. C. (2020). Automatic partial discharge recognition using the cross wavelet transform in high voltage cable joint measuring systems using two opposite polarity sensors. International Journal of Electrical Power and Energy Systems, 117. doi:10.1016/j.ijepes.2019.105695.

[45] Uwiringiyimana, J. P., Khayam, U., Suwarno, & Carlo Montanari, G. (2024). Planar Rectangular Microstrip Antenna for Partial Discharge Detection: Experimental Validation on Oil-Filled Transformer Tank. IEEE Access, 12, 133199–133208. doi:10.1109/ACCESS.2024.3459919.

[46] Kong, X., Zhang, C., Hou, C., Lin, X., & Du, B. (2024). UHF Sensor for Partial Discharge Detection Based on Coplanar Waveguide Feeding. IEEE Sensors Journal, 24(17), 28119–28128. doi:10.1109/JSEN.2024.3427412.

[47] Dimitrov, K. C., Lee, Y., Youn, J. H., Park, C. U., Oh, S. W., & Lee, M. S. (2024). Low Frequency Gain Enhancement of Cavity-Backed Electrically-Small Hybrid Spiral Antenna for High-Voltage Partial Discharge Sensing. IEEE Access, 12, 117934–117943. doi:10.1109/ACCESS.2024.3447890.

[48] Shams, M. A., Saber, E., & Gouda, O. E. (2025). Investigation of the Performance of Novel 3-D UHF Antennas for Partial Discharge Detection in Power Transformers. IEEE Sensors Journal, 25(19), 36971–36978. doi:10.1109/JSEN.2025.3598717.

[49] Chen, K., Dong, R., Meng, X., Zhu, W., & Cao, T. (2025). Research on Multiband Interference Suppression Log Periodic Antennas for Partial Discharge Detection. IEEE Sensors Journal, 25(20), 37916–37926. doi:10.1109/JSEN.2025.3605282.